



HAL
open science

Coupling of the secondary loop and the cooling circuit in a PWR involved in load follow operations

Baptiste Gasse, Jean-Michel Do, Hubert Grard, Cheikh Diop, Sébastien Verel

► **To cite this version:**

Baptiste Gasse, Jean-Michel Do, Hubert Grard, Cheikh Diop, Sébastien Verel. Coupling of the secondary loop and the cooling circuit in a PWR involved in load follow operations. PHYSOR 2022 - International Conference on Physics of Reactors 2022, May 2022, Pittsburgh (Etats-Unis), United States. pp.3304-3313. hal-03901398v2

HAL Id: hal-03901398

<https://hal.science/hal-03901398v2>

Submitted on 9 Jan 2023

HAL is a multi-disciplinary open access archive for the deposit and dissemination of scientific research documents, whether they are published or not. The documents may come from teaching and research institutions in France or abroad, or from public or private research centers.

L'archive ouverte pluridisciplinaire **HAL**, est destinée au dépôt et à la diffusion de documents scientifiques de niveau recherche, publiés ou non, émanant des établissements d'enseignement et de recherche français ou étrangers, des laboratoires publics ou privés.

COUPLING OF THE SECONDARY LOOP AND THE COOLING CIRCUIT IN A PWR INVOLVED IN LOAD FOLLOW OPERATIONS

Baptiste GASSE^{1*}, Jean-Michel DO¹, Hubert GRARD², Cheikh DIOP¹ and Sébastien VEREL³

¹ Université Paris-Saclay, CEA, Service d'Études des Réacteurs et de Mathématiques Appliquées, 91191, Gif-sur-Yvette, France.

² Institut National des Sciences et Techniques Nucléaires, CEA, 91191, Gif-sur-Yvette, France.

³ Université du Littoral Côte d'Opale, Laboratoire d'Informatique Signal et Image de la Côte d'Opale, 21 rue Saint-Louis, 62200, Boulogne-sur-Mer, France.

*Corresponding author : baptiste.gasse@cea.fr

ABSTRACT

The penetration of intermittent low-carbon energies in the French electric mix challenges the need of enhancing the flexibility of the French nuclear fleet. Most of the French nuclear reactors have been devised to do load-follow operations in order to ensure the supply and demand balance anytime. However, considering the lack of long-term high-capacity energy storage capacity, the less the share of electricity production from nuclear energy (which would be mainly compensated by the development of wind and solar energy), the more load-follow transients will be planned to manage summertime peak of electric over-production or conversely winter season peak of underproduction. A coupling between the secondary loop and the cooling circuit of a pressurized water reactor has been implemented in addition to a simulator oriented 1300 MW reactor model. We present here our modeling of the steam turbines, the moisture separator, the water reheater and the condenser for a typical 1300 MW P⁴ stage provided with an open-loop cooling circuit. As we study off-design load conditions, we simulate a load transient based on real electricity production profile done in the past few years. We compare the cold source water heating downstream of the plant measured on site and the one we calculate with our secondary loop and cooling circuit.

KEYWORDS: PWR, secondary loop, cooling circuit, thermodynamics.

1. INTRODUCTION

The performance of the nuclear fleet is strongly linked with its ability to follow the load demand daily. It can be self-regulating power variations around $\pm 7\%$ of a reactor's nominal power (NP) when the network's frequency slightly deviates from the setpoint (remote-tuning plus secondary adjustment of frequency), or load follow operations making the reactor power decrease from baseload mode to a power value less than $92\%NP$ and greater than a limit of nearly $30\%NP$. These load follow maneuvers are limiting at the scale of a reactor core as it makes the xenon concentration change as well as the axial power distribution, which affect for a few hours the stability of the core. A quick back to baseload mode just after the decreasing power ramp can be prevented under some conditions because by the pellet-clad interaction, for instance.

Also, climate change must be taken into account as it can alter nuclear reactors maneuverability. For instance, global warming make the temperature of nuclear reactor cold source higher, which leads to a loss of the plant efficiency [1]. In this paper, we present a coupling of the secondary circuit with the cooling circuit. The first converts the core thermal energy into rotational kinetic energy through steam turbines while the second is necessary to condense the vapor coming out of the low pressure (LP) turbine. We model an open cooling circuit, which means that the cold water withdrawn from the river or the sea to pass through the condenser's tubes is entirely restored to the environment. We will focus on the heat exchange occurring in the condenser warms up the cold source water between the upstream and the downstream of the NPP: this parameter is under supervision at all times to prevent that water heating exceeds the limits imposed by French environmental laws.

2. DESCRIPTION OF THE MODELING FOR THE SECONDARY CIRCUIT

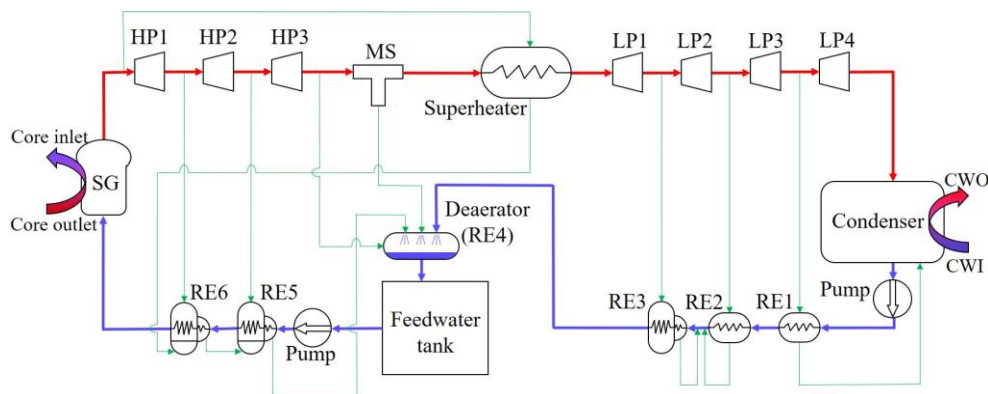


Figure 1. Schematic of the secondary circuit

Figure 1 introduce the global loop model for the coupling. It is compliant with the technology of French P'4 1300 MW nuclear reactors. The steam generator (SG) generates dry steam thanks to heat exchange with the primary fluid of the reactor. Then it passes through the turbines to deliver a great amount of its thermal power into kinetic energy. Let η be the efficiency of the power plant : $\eta\%$ of the thermal power extracted thanks to nuclear fission is converted effectively into raw power production, whereas roughly $(1 - \eta)\%$ of the thermal power is released to the cold source to the level of the condenser (second law of thermodynamics). Water reheaters are commonly used in power plants to improve the thermodynamic efficiency of the Rankine cycle, as they enable to heat feedwater before it returns into the steam generator. This circuit is simplified compared to reality, but it addresses complex connections between each component to simulate a consistent physical behavior to study baseload and load following modes of production. Similar schematic Rankine loop has already been used to carry out interesting studies such as the optimization of mass flow regulation at turbine extraction stages [2] or the improvement of water reheater's efficiency and the turbines behavior for off-design load conditions [3-4].

2.1. The turbines

In our model, HP turbine and LP turbine only differ by the number of steam extraction stages. Hereafter we call *turbine stage* a group of bladings in between a steam inlet and outlet (thus HP turbine has three stages whereas LP turbine has four stages). We use the same model for both turbines. It consists in calculating the specific enthalpy at the outlet of a turbine stage for a given value of net electrical output of the plant. Firstly we find steam entropy at the outlet considering an ideal turbine, thanks to steam tables [5] and steam

*Making Virtual a Reality: Advancements in Reactor Physics To Leap Forward Reactor
Operation and Deployment*

properties at the inlet (pressure and enthalpy). Secondly, we use (1) to find steam non-isentropic specific enthalpy at the outlet. Not only we assume that mechanical work produced by HP and LP turbine keeps the same proportion during baseload mode and off-design load dynamic conditions, but it is also the case for each HP and LP stages. Parameters C^α and C^β represent the contribution of each turbine and stages respectively and were adapted from [6]. Their values are given in table I. We don't consider kinetic loss at the outlet of the LP turbine, which means that the whole produced mechanical power should be attributed to the enthalpy drop due to steam expansion. Also, we consider in our model 2MW of mechanical loss, 60MW of electrical power used for the plant's own electrical circuits and an efficiency of mechanical to electrical power conversion of 99%.

$$h_o^{\text{stage}} = h_i^{\text{stage}} - \frac{C^{\text{stage}}}{\dot{m}_{\text{stage}}} P_{\text{mecha}} \quad \text{with } P_{\text{mecha}} = \left(\frac{P_{\text{elec}} + 60\text{MW}}{0.99} + 2\text{MW} \right) \text{ and } C^{\text{stage}} = C^\alpha C^\beta \quad (1)$$

Table I. Contribution of each turbine stage for mechanical power. Adapted from [6].

	HP turbine			LP turbine			
P_{mecha} (MW)	496,9			907,5			
C^α	35,8%			64,2%			
	HP1	HP2	HP3	LP1	LP2	LP3	LP4
P_{mecha} (MW)	232,5	125,5	138,9	287,7	271	204,8	144
C^β	47%	25,3%	27,7%	31,7%	29,9%	22,5%	15,9%

We've calculated steam entropy for an ideal turbine and steam non-isentropic enthalpy at the outlet. Finally, we need to get steam isentropic enthalpy in order to find steam pressure at the outlet of the turbine stage. To do so we consider equation (2) which defines isentropic efficiencies $\eta_{\text{is}}^{\text{stage}}$ of each turbine stage:

$$h_o^{\text{is, stage}} = h_i^{\text{stage}} - \frac{h_i^{\text{stage}} - h_o^{\text{stage}}}{\eta_{\text{is}}^{\text{stage}}} \quad (2)$$

Furthermore, the more the load diminishes the more the loss of entropy through a stage during the steam expansion, which is a behavior frequently encountered in power plants [7-9]. We consider that the isentropic efficiency decrease of around 2% between baseload mode and half-load mode [8], and we choose a linear evolution from 100%NP to 30%NP given by these two reference points (table II). Values for the 100%NP reference point are taken from [9] for a French P'4 1300 MW NPP.

Table II. Reference values for the variation of efficiency of turbine stages. Adapted from [8, 9].

Turbine stages	HP1	HP2	HP3	LP1	LP2	LP3	LP4
$\eta_{\text{is}}^{\text{stage}}$ (100%NP)	86%	82%	79%	91%	90%	87%	89%
$\eta_{\text{is}}^{\text{stage}}$ (50%NP)	84.4%	80.5%	77.5%	89,3%	88,3%	85,4%	87,4%

Pressure at the outlet is calculated with the help of IAPWS-97 water tables [5] considering $S_o^{\text{is, stage}}$ and $h_o^{\text{is, stage}}$. This pressure given for an ideal transformation is the same as for a non-isentropic one. We deduce steam temperature at the outlet from pressure and h_o^{stage} .

2.2. The moisture separator (MS)

Steam expansion in HP turbine affects steam humidity. During baseload mode, the steam quality is around 89% at the outlet of HP turbine, which is enough to damage the LP turbine pale because of the steam speed. The moisture separator (MS) prevents this by separating liquid and vapor phases. We model the MS by

combining a mass balance (3) and an energy balance (4) through the component. We neglect pressure and thermal loss during the transformation.

$$\dot{m}_i = \dot{m}_o^l + \dot{m}_o^v, \text{ with } \begin{cases} \dot{m}_o^l = (1 - x_i)\dot{m}_i \\ \dot{m}_o^v = x_i\dot{m}_i \end{cases} \quad (3)$$

$$\dot{m}_i h_i = \dot{m}_o^l h_o^l + \dot{m}_o^v h_o^v \quad (4)$$

2.3. The superheater

The steam superheater overheats the main circuit steam coming from the HP turbine (whose steam quality is 100% thanks to the MS). A fraction of the steam extracted from the SG is withdrawn to state as the *hot* fluid for the overheating process. It is assumed that the vapor withdrawal rate of the SG is equal to 9,5% of all the steam generated at all loads (there is no valve regulation for this withdrawal branch in between 30%NP and 100%NP [9]). In our model, we suppose that the heat transmitted to the *cold* steam (the one that will enter the LP turbine) is such that the *hot* fluid condenses totally (thus the superheater states as a condenser component). At the *hot* fluid outlet, the enthalpy of the liquid is equal to the saturated liquid enthalpy. Again, we neglect heat and pressure losses in this component at all loads so that the superheater is ideal (in 1984, heat losses represented about 9% of global heat exchanges on Saint-Laurent NPP [10]).

2.4. The feedwater reheaters

Heat exchanges in the feedwater reheaters are used to calculate the mass flow extracted from turbine stages by inversion. In our modeling, the steam flow withdrawn from a turbine stage enables to state the new steam flow rate at the inlet of the next stage. We use a dynamic curve based on real measurement made on a French P4 1300MW NPP [6] that gives the water heating through the file of low pressure and high pressure water reheaters (RE1, RE2, RE3, RE4 and RE5, RE6 respectively, cf. figure 1) between 30%NP and 100%NP. Having access to such measurement simplifies thermal calculation in each reheater cavity, which normally depends on the pressure and the level of water [3]. During a load transient, it frequently happens that both of these parameters shift, hence a modification of the heat transfer coefficient. We do not consider these variations in our study because a setpoint regulates the cavity pressure and the water level automatically. In our model, heat exchanges that occur inside a solely reheater must be known in order to calculate the steam mass flow extracted at each turbine stages by applying an energy balance. We choose to evaluate during baseload mode production the contribution of each reheater for the global heating. Namely, we use steam flow at turbine extraction branches given in [9] to evaluate heat transfer in each reheater. These contributions are indexed in table III and we assume they are constant with load conditions.

Table III. HP and LP reheater contribution to the global water heating right after the condenser.

Reheater	RE1	RE2	RE3	RE4	RE5	RE6
Contribution	15,8%	21,7%	28%	34,5%	48,1%	51,9%

2.4.1. Single zone reheater (condensation)

The feedwater reheaters RE1 and RE2 are the simplest one to manage as we model them with a single condensation zone. Equation (5) is a classic energy balance which gives the steam mass flow rate to match heat exchanges given at all load by the dynamic heat exchanges curves published in [6].

$$\dot{m}^h (h_i^h - h_{\text{sat}}^h) = \dot{m}^c (h_o^c - h_i^c). \quad (5)$$

2.4.2. Two-zone reheater in addition with additional bleed inlet

We model both RE5 and RE6 reheater with a *condensing zone* and a *drain cooling zone (DC zone)*. When the cold water gets into the reheater U-shaped tubes, it firstly heats up in the DC zone (modelled as a liquid-liquid heat exchanger) then it gains the heat of the hot steam condensation in the condensation zone.

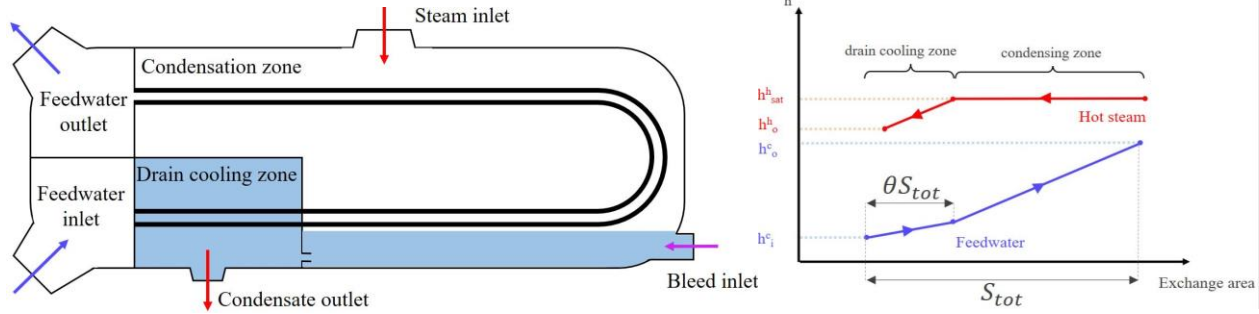


Figure 2. Schematic of our modelling of a two-zone reheater with additional bleed inlet (left) and a representation of its heat exchange diagram (right).

The drain consists in condensed *hot steam* (steam that came from the turbine extraction stage) as well as condensates from the superheater (for RE6) or from RE6 bleed outlet (for RE5). We introduce a schematic view of such a reheater in figure 2 (left). We model separately and successively the two zones as they call on different heat transfer coefficient (figure 2, right). We assume that for both RE5 and RE6 reheaters bleed inlets are always liquid whatever the reactor load. We use an energy balance (6) to describe heat exchanges in the condensation zone that involves a known final state (indeed, thermodynamic properties of the fluid are known thanks to dynamic curves of T_{ADG} and T_{ARE} with load published in [6]) and a fictive unknown state, the one that defines the feedwater properties after its passage through the DC zone.

$$\dot{m}^h (h_i^h - h_{sat}^h) = \dot{m}^c (h_o^c - h_m^c) \quad (6)$$

with h_m^c the enthalpy of cold fluid right after the DC zone in the liquid-liquid exchanger. Equation (6) shows two unknown variables : h_m^c and \dot{m}^h , the steam mass flow of the hot fluid whose calculation is the main purpose of this model because it is also the steam mass flow rate of turbine extraction stage. As the liquid-liquid heat exchanger is a fictive representation of a two-zone reheater, we cannot validate the fluid state afterwards the calculations thanks to industrial charts. Some authors use iterative calculations limited by physical industrial constraints [2] or use the Delaware method to estimate the heat transfert coefficient in each zone in order to get another equation involving \dot{m}^h and finally find it [3]. The first method was not adapted for our model since we want to implement the coupling into a pre-existing simulator oriented PWR model [11] and an iterative procedure is too long to proceed a simulation in a short amount of time. The second method assume that we have some datas depicting the reheater cavity and piping dimensions, which is not the case here. Therefore we fix the contribution of the fictive DC zone for the global feedwater heating with the help of baseload mode charts provided in [9]. This contribution is given in table IV.

Table IV. Contribution of the drain cooling zone for global feedwater heating for each HP reheater.

High pressure reheater	RE6	RE5
Contribution of the drain cooling zone (θ parameter)	30,6%	17,8%

For instance if the feedwater gains 300 kJ/kg through RE6 it means that 91,8 kJ/kg (30,6% of the rise) owes the heat exchange in the DC zone. Some research has demonstrated that the level contribution of the DC

zone (which physically stands for the liquid-liquid heat exchange area) varies with hot steam pressure and mass flow variations [12]. The study shows there is shift of this contribution when hot steam pressure passes from 2,7 MPa to 3,8 MPa. Thus, hot steam heat exchanges with feedwater in the DC zone progressively overtake the one through the condensation zone during such a transition. Conversely, the more the hot steam flow rates the less the contribution of the DC zone. In our model, we consider that pressure variation effects cannot overtake the importance of steam flow rates involved even during a load transient. Therefore, we assume contributions presented in table IV are constant with load variations. Finally, we calculate the hot steam needed to be extracted at turbine stages to respect the dynamic feedwater heating curve taken from industrial measurements thanks to equation (7). Then the enthalpy of the condensates needed for the next reheater are given by equation (8).

$$\dot{m}^h = \dot{m}^c \frac{(h_o^c - h_i^c)(1 - \theta)}{h_i^h - h_{sat}^h} \quad (7)$$

$$h_o^h = \frac{\dot{m}^h h_{sat}^h + \dot{m}^b h_i^b - \dot{m}^c (h_o^c - h_i^c) \theta}{\dot{m}^h + \dot{m}^b} \quad (8)$$

2.4.3. Two-zone reheater with no drain cooling zone

We model RE3 feedwater reheater with both same heat exchange zones that the ones presented in previous section except that there is no additional bleed inlets arriving in the DC zone. Heat exchanges through RE3 are modelled as introduced in figure 2 but equation (8) is slightly different (no *bleed* terms).

2.4.4. Single zone reheater with bleed inlets : the deaerator / RE4

The deaerator is a component that prevents non-condensable gases to reach the steam generator so that corrosive effects are limited on the long term [2, 6]. We assimilate it as the final low-pressure heat exchanger that connects four main branches: the feedwater representing the *cold fluid* in heat exchangers philosophy, and *hot fluids* represented by HP turbine last extraction and RE5 bleed water and moisture separator respective condensates [2]. The modeling of the deaerator enables to calculate the steam flow rate extracted after HP turbine and just before the moisture separator. Again, we use an energy balance (9) but because the flow rate of feedwater is still unknown at this step of the loop (*cf.* fig.1), the equation that gives \dot{m}^c is more complex (10).

$$\dot{m}_{HP3}^{ext} h_{HP3}^{ext} + \dot{m}_{RE5} h_{RE5} + \dot{m}_{MS} h_{MS} + \dot{m}_{RE3} h_{RE3} = \dot{m}_{FWT} h_{FWT} \quad (9)$$

$$\dot{m}_{HP3}^{ext} = \frac{\dot{m}_{RE5}(h_{RE5} - h_{FWT}) + x_{HP3} \dot{m}_{HP3}(h_{RE3} - h_{MS}^{sat}) + \dot{m}_{HP3}(h_{MS}^{sat} - h_{FWT})}{(1 - x_{HP3})h_{MS}^{sat} + x_{HP3}h_{RE3} - h_{HP3}^{ext}} \quad (10)^1$$

2.5. The condenser

The condenser carries away around two thirds of the reactor core thermal power at all loads. Therefore, the efficiency of the whole reactor strongly depends on the efficiency of the condenser. Heat exchanges that occur in the condenser of reactors provided with an open loop cooling circuit involve a water withdrawal from the river or seawater, whose temperature depends of weather conditions. In France, the temperature of such cold source tends to increase progressively, and low water levels (that directly affects the flow rate of the cold source) happen regularly because of recurrent summer heat waves [13]. The hotter the cold

¹ Nomenclature of all terms is given at the end of this paper.

Making Virtual a Reality: Advancements in Reactor Physics To Leap Forward Reactor Operation and Deployment

source temperature, the less the efficiency of the NPP. Indeed, not only a rise in the temperature of the cold source deteriorates heat exchanges between the *cold water* and the steam coming from the LP turbine [14], it also affects the performance of the LP turbine [15]. Furthermore, the condenser's cavity saturated pressure also depends on the load. Condenser's vacuum pumps are usually devised with a curve network that gives the dependence with load, cold source temperature and flow rate through condenser's tubes of the saturated pressure at which heat exchanges occur [16]. As we do not have access to such industrial specifications, we've created a web of curves based on common datas published in the literature [14, 16]. The web aims at fixing saturated pressure of condenser's cavity with a given triplet of values : current load of the plant, cold source temperature and cold source volumic flow rate. In our study, we consider that the pressure is homogeneous in the cavity (in reality, pressure drop occur in the cavity vertically). It is presented on figure 3 (left). Furthermore, a variation of cold source temperature directly affects the thermal efficiency of the plant. Our load follow simulator [11] originally used a single curve giving the real thermal efficiency with load, which have been calculated by EasyREP® in [6] (figure 3, right, curve at 15°C). For the needs of our model, we use a web of thermal efficiency curves by slightly adjusting thermal efficiency variations proportionally to variations of Carnot's efficiency with a changing cold source temperature (in percentage points per °C). Results are presented on figure 3 (right).

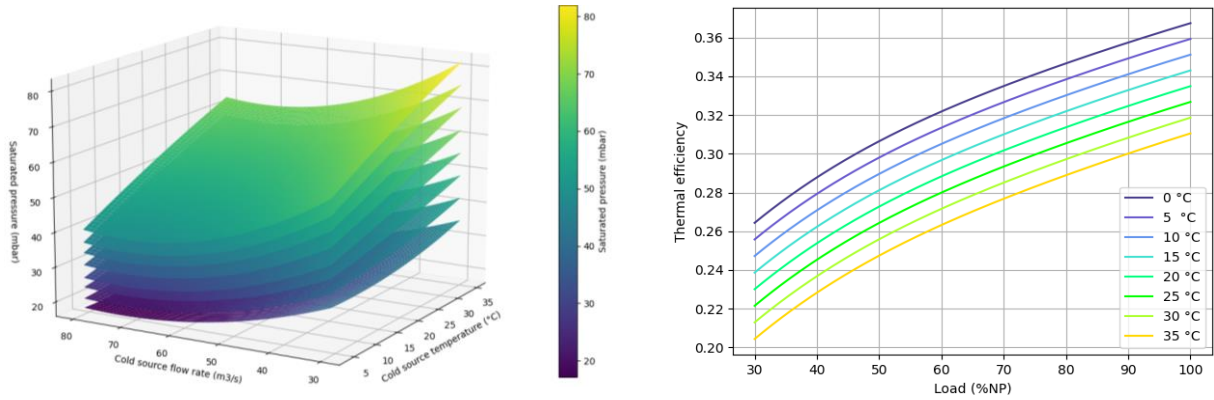


Figure 3. Left : saturated pressure curves in condenser's cavity (left). Each plane stands for an “iso-load” plane (100%PN at the top and 30%PN at the bottom). **Right :** web of curves giving the global loss of efficiency of the NPP due to a hotter cold source.

We calculate $T_{\text{cond. output}}$, the cold water temperature at the outlet of the condenser with equation (11) :

$$T_{\text{cond. output}} = T_{\text{cond. inlet}} + \frac{\dot{m}^h (h_i^h - h_{\text{sat}}^h)}{Q_{\text{condenser}} C_p^c} \quad (11)$$

where C_p^c is the mean value of cold water specific heat at $T = 0.5 * (T_{\text{cond. output}} + T_{\text{cond. inlet}})$ and $P = 1$ bar.

3. RESULTS

Our study aims at finding the cold source temperature heating through the condenser in modeling real load following operations done in 2019 and 2020 on two P4/P'4 NPP stages. We use production profiles as an input in our model, which is flattened compared to the one given by RTE on its website [20]. Namely, we take the mean electricity production during periods only affected by frequency remote control ($\pm 7\%$ NP), and we model load drops that happen casually during a month. Figure 4 shows an example of such a transient. The cold water flow rate that pass through the condenser is given by annual reports made by EDF [18] for each NPP under study. In this reports, EDF gives the cold source temperature upstream the NPP. Here we use datas provided from St-Alban and Penly NPPs (2 reactors, stage P'4 for both of them). One must note that the Rhône (a French river) cools the first one whereas the other one is built on the French

North-West coast so that it's cooled by seawater. Finally, we calculate cold water heating through the condenser. For St-Alban NPP we compare the river heating between upstream and downstream the NPP after the mixing of water coming from the condenser with the main arm of the river with the hall of equation (13). We use flow rates measured by the hydraulic station of Ternay [19]. For Penly, EDF report gives

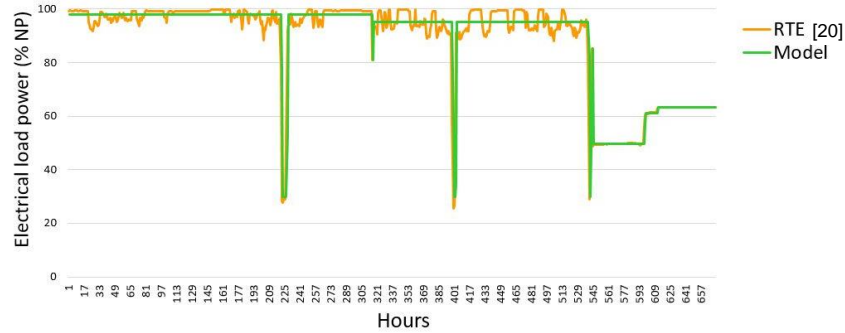


Figure 4. Production profile made by St-Alban P'4 first reactor in February 2019 (orange), and our model used as input for the simulation (green).

directly the water heating of water at the discharge well, so that we can compare the water heating before and after water pass through cross the condenser. The results of our simulations are given in figure 5. We fix the mass flow rate through the condenser's tube $Q_{\text{condenser}}$ by applying equation (12) that uses of the monthly volume of water withdrawn from the river or seawater measured by EDF [18], noted V_m .

$$Q_{\text{condenser}} = \frac{V_m}{\text{seconds per month}} \cdot \frac{1}{\text{Nb of working units in NPP}} \quad (12)$$

For instance, if $V_m = 339 \cdot 10^6 \text{ m}^3$ (amount of water withdrawn from the river during June 2019 for St-Alban NPP), we use $Q_{\text{condenser}} = 65,394 \text{ m}^3/\text{s}$ as an input for the cold source flow rate in our model.

$$T_{\text{downstream}} = \frac{Q_{\text{cond.}} \cdot \sum (Cp \cdot T)_{\text{cond. output}}^{\text{unit } i} + (Q_{\text{main arm}} - 2Q_{\text{cond.}}) Cp_{\text{main arm}} T_{\text{main arm}}}{(Q_{\text{main arm}} - 2Q_{\text{cond.}}) Cp_{\text{main arm}} + Q_{\text{cond.}} \cdot \sum Cp_{\text{cond. output}}^{\text{unit } i}} \quad (13)$$

One should notice that we cannot simulate all months of year 2019 and 2020. Indeed, as our simulator can't model the behaviour of the reactor core at thermal power load below 30% NP, we can't study a month when a load drop below 30%NP occurs. Also, EDF reports of St-Alban and Penly NPP give a monthly water volume withdrawn from the cold source to cool reactors. As a reactor that stops electricity production still needs to be cooled because of thermal residual power, it still receives cold source water, but there is a great uncertainty over the term "number of working units in NPP" in equation (12) when one reactor of the NPP stops during a whole month.

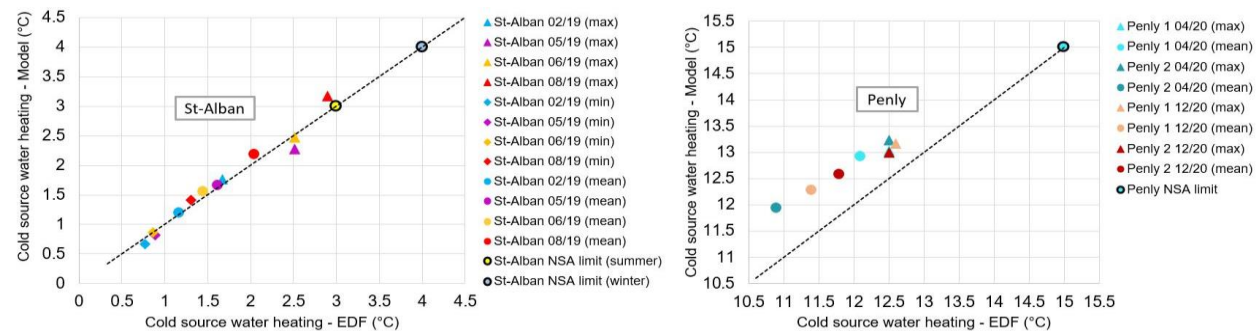


Figure 5. Cold source water heating corresponding to production profiles of St-Alban NPP (left) and Penly NPP (right). Comparison between EDF measurements [18] and the load follow simulator.

*Making Virtual a Reality: Advancements in Reactor Physics To Leap Forward Reactor
Operation and Deployment*

Results shows our model of the secondary loop gives good consistency with water heating datas from EDF report for St-Alban NPP. However, results for Penly NPP show our model provides a good tendency for the evolution of water heating for different month of the year, but comparisons with EDF report's water heating datas are mediocre. A possible explanation could be that we've devised our model by considering thermodynamic properties of industrial documents published in [9] that were taken from St-Alban P'4 NPP exploitation, and we extend the use of this model to Penly NPP. However, even though its secondary loop are both P'4 stage, results show such an extend of the model should be taken with caution. It seems that we must calibrate the web of curves giving the saturated pressure in the condenser's cavity to get good consistency with EDF's Penly measurements, instead of using the same web of curves for both NPPs. Also, the nature of the cooling source can affect the fouling factor of condenser's tubes. Moreover, a reactor cooled by seawater is more likely to get obstructed tubes than a reactor cooled by a river with no salinity. In our study, we don't consider any fouling factor, but it can be non-negligible in some NPP ; it affects the heat transfer coefficient (on the inner wall of the tubes), and in the end the pressure in the condenser's cavity. Our study invites to refine our model by choosing a more adapted web of curves for condenser's cavity (figure 3) for Penly NPP. In addition, results obtained for St-Alban NPP show good consistency not only for the mean water heating over a month, but also for the minimal and maximal values measured on the same period. It leads us to consider that our model is as robust during baseload mode as during events of load following mode. Finally, in St-Alban NPP, water heating after mixing with the main river branch must not exceed 4°C during winter season and 3°C during summer season. These limits are less restrictive for NPPs at the seaside, as it must not exceed 15°C at all time.

4. CONCLUSIONS

We have devised a simplified non-linear model for the coupling of a French P'4 1300MW pressurized water reactor cooling circuit with its secondary loop, in addition to a pre-existent validated simulator itself coupling primary circuit with the secondary loop [11]. We have simulated real historical production profiles during a whole month that involves several load transient that our simulator can handle. The coupling we've modeled shows good consistency with measurement datas to reproduce the behavior of load follow operations towards the cold source water heating. This coupling could be use in a future work to design new constraints for an optimization study dealing with a reactor maneuverability that takes into account temperature and flow rate of the cold source (river or seawater).

NOMENCLATURE

$\dot{m}_i (h_i)$: fluid mass flow rate (enthalpy) at the inlet.
$\dot{m}_0 (\dot{m}_0^l, \dot{m}_0^v)$: fluid (liquid phase, vapor phase of the fluid) mass flow rate at the outlet.
$h_0 (h_0^l, h_0^v)$: fluid (liquid phase, vapor phase of the fluid) enthalpy at the outlet.
$\dot{m}^h (\dot{m}^c)$: mass flow rate of hot fluid (cold fluid) in heat exchanger formalism.
$h_i^h (h_i^c)$: enthalpy of the hot fluid (cold fluid) at the inlet in heat exchanger formalism.
$h_o^h (h_o^c)$: enthalpy of the hot fluid (cold fluid) at the outlet in heat exchanger formalism.
h_{sat}^h	: saturated liquid enthalpy of the hot fluid in heat exchanger formalism.
θ	: contribution of the drain cooling zone for heat exchanges model of RE5 and RE6.
h_m^c	: enthalpy of the cold fluid at the outlet of the drain cooling zone (for RE5 and RE6 only).
$\dot{m}^b (h_i^b)$: bleed masse flow rate (enthalpy) at the inlet.
$\dot{m}_{HP3}^{ext} (h_{HP3}^{ext}, x_{HP3})$: mass flow rate (enthalpy, steam quality) of the steam extracted after HP3 stage.
$\dot{m}_{RE5} (h_{RE5})$: condensate mass flow rate (enthalpy) at the outlet of RE5.
$\dot{m}_{MS} (h_{MS}, h_{MS}^{sat})$: condensate mass flow rate (enthalpy, saturated liquid enthalpy) at the outlet of the MS.
$\dot{m}_{RE3} (h_{RE3})$: feedwater mass flow rate (enthalpy) at the outlet of RE3.

$\dot{m}_{\text{FWT}} (h_{\text{FWT}})$: feedwater mass flow rate (enthalpy) at the inlet of the feedwater tank (cf. figure 1).

ACKNOWLEDGMENTS

The authors would like to thank INREL, a project of CEA GEN2&3 program, for their financial support.

REFERENCES

1. S. I. Attia, "The influence of condenser cooling water temperature on the thermal efficiency of a nuclear power plant," *Annals of Nuclear Energy*, **80**, pp. 371-378 (2015).
2. A. Teyssedou, J. Dipama, W. Hounkonnou and F. Aubé, "Modeling and optimization of a nuclear power plant secondary loop," *Nuclear Engineering and Design*, **240**(6), pp. 1403-1416 (2010).
3. M. Álvarez-Fernández, L. del Portillo-Valdés and C. Alonso-Tristán, "Thermal analysis of closed feedwater heaters in nuclear power plants," *Applied Thermal Engineering*, **68**(1-2), pp. 45-58 (2014).
4. M. Álvarez-Fernández, L. del Portillo-Valdés and C. Alonso-Tristán, "Thermal balance of wet-steam turbines in nuclear power plants : a case study," *Applied Thermal Engineering*, **93**, pp. 598-605 (2016).
5. W. Wagner and H. J. Kretzschmar, *International Steam Tables: Properties of Water and Steam Based on the Industrial Formulation IAPWS-IF97*, Springer, Berlin, Germany (2008).
6. H. Grard, *Physique, fonctionnement et sûreté des REP: Le réacteur en production*, EDP Sciences (2014).
7. A. S. Karakurt and Ü. Güneş, "Performance Analysis of a Steam Turbine Power Plant at part Load Conditions," *Journal of Thermal Engineering*, **3**(2), pp. 1121-1128 (2017).
8. A. Ray, "Dynamic modelling of power plant turbines for controller design," *Applied Mathematical Modelling*, **4**(2), pp. 109-112 (1980).
9. S. Marguet, *La technologie des réacteurs à eau pressurisée*, EDP Sciences (2019).
10. G. Bell and A. R. Wazzan, "Thermal hydraulic performance of a moisture separator reheater at the 900 MWe PWR Saint Laurent Unit B1," *Nuclear Engineering and Design*, **85**(3), pp. 363-372 (1985).
11. V. Drouet, J.-M. Do, S. Vérel and J.-C. Le Pallec, "Design of a simulator oriented PWR model and optimization of load-follow operations," *International Conference on Physics of Reactors: Transition to a Scalable Nuclear Future (ICAPP 2019)*, Juan-les-Pins, France (2019).
12. I. S. Hussaini, S. M. Zubair and M. A. Antar, "Area allocation in multi-zone feedwater heaters," *Energy Conversion and Management*, **48**(2), pp. 568-575 (2007).
13. S. Ibrahim, M. Ibrahim and S. I. Attia, "The Impact of Climate Changes on the Thermal Performance of a Proposed Pressurized Water Reactor: Nuclear-Power Plant," *International Journal of Nuclear Energy*, **2014**, pp. 1-7 (2014).
14. M. Laković, M. Stojiljković, S. V. Laković, V. P. Stefanović and D. Mitrović, "Impact of the cold end operating conditions on energy efficiency of the steam power plants," *Thermal Science*, **14**(suppl.), pp. 53-66 (2010).
15. W. H. Al-Taha and H. A. Osman, "Performance Analysis of a Steam Power Plant: A Case Study," *MATEC Web of Conferences*, **225** (2018).
16. W. Lévy, "Condenseurs par surface dans les centrales thermiques," *Techniques de l'Ingénieur*, **B1540**(V1) (1990).
17. A. Žukauskas, "Heat transfer from tubes in crossflow," *Advances in Heat Transfer*, **8**, pp. 93-160 (1972).
18. EDF, *Rapport environnemental annuel relatif aux installations nucléaires du CNPE de Saint-Alban* [resp. Penly], (2019 and 2020) [resp. (2020)].
19. CN Rhône, *Débits journaliers et mensuels du Rhône – station de Ternay*, HYDRO-MEDDE/DE (2019).
20. "Production réalisée par groupe," <https://www.services-rte.com> (2019 and 2020).